Device

CellPress
OPEN ACCESS

Review

# Life-cycle assessment of carbon footprint and energy intensity of thermoelectric generator production for near-room-temperature applications

Amir Pakdel[1,*] and Alex Reilly[1]
[1]School of Engineering, Trinity College Dublin, The University of Dublin, D02 PN40 Dublin, Ireland
*Correspondence: pakdela@tcd.ie
https://doi.org/10.1016/j.device.2026.101085

**THE BIGGER PICTURE** By converting waste heat directly into electrical power, thermoelectric generators (TEGs) can improve the energy efficiency of fossil fuel/thermal power stations. Although TEGs produce electricity without direct carbon emissions, their overall sustainability remains uncertain once the energy- and resource-intensive nature of their manufacturing is considered. Processes such as rare metal extraction, element refining, alloy synthesis, device fabrication, and disposal can significantly offset the environmental benefits of waste-heat recovery. With commercial devices operating at <5% efficiency, energy payback times (EPBTs) may extend beyond practical lifetimes. In this review, we present a process-resolved, device-level life-cycle baseline for $Bi_2Te_3$-based TEGs, linking manufacturing energy and emissions to delivered electrical output through energy and carbon payback metrics.

## SUMMARY

Thermoelectric generators (TEGs) can generate clean electricity from waste heat, but their production also generates energy demand and greenhouse gas (GHG) emissions. In this work, we analyze the time it takes for a TEG to earn back the input energy invested in its manufacturing and the time it takes to offset the associated $CO_2$ emissions. At $\Delta T = 30^{\circ}C$, the energy payback time (EPBT) ranges from 2.7 to 8.2 years but can fall to 0.5–1.5 years at $\Delta T = 70^{\circ}C$. The global warming potential (GWP) per module ranges from 0.80 to 1.51 kg $CO_2$ equivalent ($CO_2$-equiv). Offsetting this climate burden requires continuous operation at $\Delta T = 30^{\circ}C$ for 1.2–3.1 years, but the offset period drops to less than 2 months if renewable electricity is used. Our analysis concludes that powder metallurgy synthesis routes and renewable electricity supplies are critical levers to reduce EPBT and $CO_2$ offset times. Optimization of tellurium use and promotion of its recycling can further mitigate non-climate burdens.

## INTRODUCTION

The search for sustainable and clean energy technologies has intensified due to the increasing global demand for electricity, coupled with the urgent need to mitigate climate change. Among the many emerging options, thermoelectric generators (TEGs) have attracted attention due to their ability to convert waste heat directly into electrical power. By harvesting otherwise lost thermal energy, TEGs offer a pathway toward improving overall energy efficiency and reducing greenhouse gas (GHG) emissions.[1] TEGs operate based on the Seebeck effect, a phenomenon wherein a temperature gradient across dissimilar conductors or semiconductors generates a voltage. In a typical TEG module, n-type and p-type semiconductor legs are sandwiched between two ceramic plates and electrically connected by metallic plates, as shown in Figure 1A. When the two sides are exposed to different temperatures, charge carriers (electrons in the n-type and holes in the p-type legs) migrate from the hot side to the cold side, resulting in an electric current.[2]

TEGs offer several key advantages, including direct energy conversion with no intermediate mechanical stage (unlike conventional heat engines); no moving parts or working fluids, which minimizes maintenance and operational complexity; silent operation and flexible installation orientation; scalability, ranging from microscale power generation to multi-kilowatt systems; and long operational lifespan, especially when coupled with steady heat sources.[3] Despite these benefits, TEGs' adoption has been limited by their low conversion efficiency. The performance of thermoelectric (TE) materials can be quantified by the dimensionless figure of merit $ZT$, defined as $ZT = \frac{\sigma S^2}{\lambda} T$, where $S$ is the Seebeck coefficient, $\sigma$ the electrical conductivity, $\lambda$ the thermal conductivity, and $T$ the absolute temperature. The energy

Please cite this article in press as: Pakdel and Reilly, Life-cycle assessment of carbon footprint and energy intensity of thermoelectric generator production for near-room-temperature applications, Device (2026), https://doi.org/10.1016/j.device.2026.101085



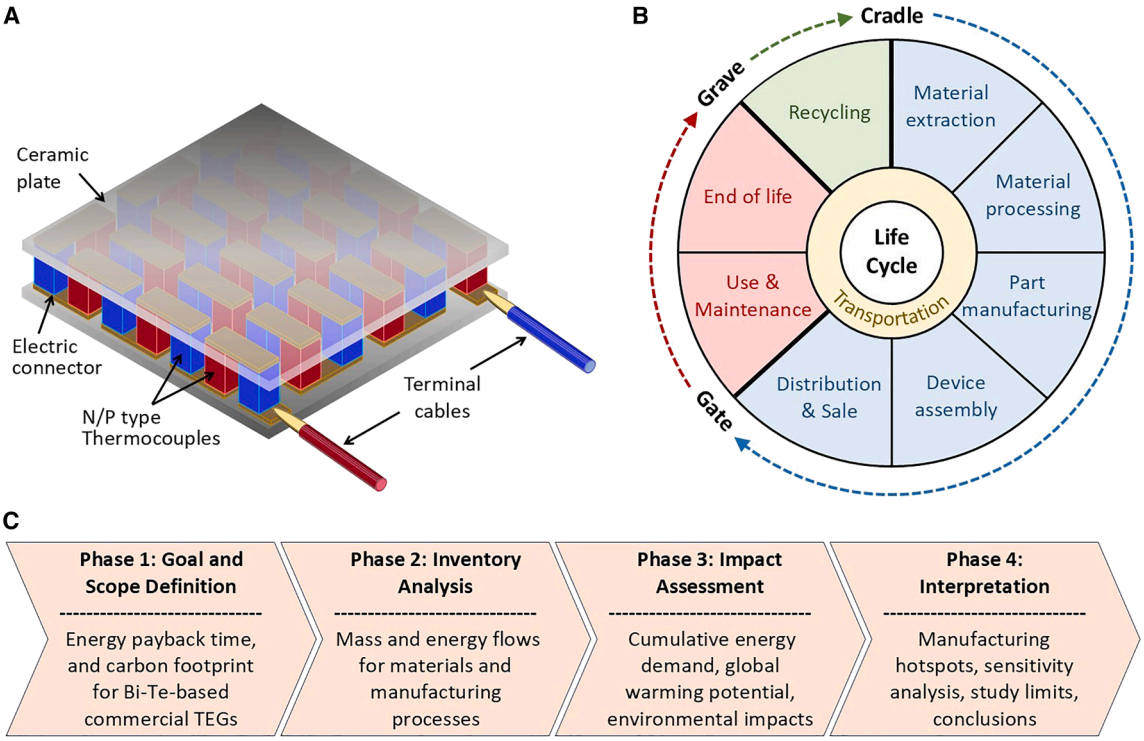


**Figure 1. Device architecture, study scope, and LCA roadmap**

(A) A schematic of a commercial TEG and its components, including p/n-type thermoelectric legs made of $Bi_2Te_3$, electric connectors made of Cu, ceramic plates made of $Al_2O_3$, and terminal cables made of Cu or Al covered by polyvinyl chloride (PVC) or rubber.

(B) ISO 14040 context and life-cycle phases. The blue dashed line indicates the cradle-to-gate boundary adopted here (transport included). The red and green dashed lines indicate cradle-to-grave and cradle-to-cradle boundaries, respectively, for context.

(C) ISO 14040 roadmap linking the four ISO phases to this study (details in the results and discussion).

conversion efficiency ($\eta$) of a TEG is a function of the average $ZT$ of the materials and the temperature difference ($\Delta T$) across the device, given by $\eta = \frac{\Delta T}{T_h}\frac{\sqrt{ZT_{avg}+1}-1}{\sqrt{ZT_{avg}+1}+\frac{T_c}{T_h}}$, where $T_h$ and $T_c$ are the temperatures of the hot and cold sides, respectively.

In the near-room-temperature regime (≈300 K), bismuth telluride ($Bi_2Te_3$)-based alloys and compounds are known to demonstrate the highest $ZT$ among other TE materials, typically $ZT \approx 0.8$–$1.1$. In practice, a $ZT \approx 1$ is regarded as a baseline for meaningful device performance at modest $\Delta T$, whereas materials with a $ZT$ of <0.5 yield limited conversion efficiency unless $\Delta T$ is very large. Currently, commercial TEGs for near-room-temperature applications contain $Bi_2Te_3$-based TE materials with $ZT \approx 1$, resulting in device efficiencies of ~5% under practical conditions (e.g., at $T_c$ = 300 K and $T_h$ = 450 K). More broadly, TEG efficiency is fundamentally limited by the Carnot efficiency ($\Delta T/T_h$); thus, even with improved $ZT$, conversion efficiencies remain modest for low-grade temperature differences. Research advances in nanostructuring, nanocompositing, and quantum confinement have pushed $Bi_2Te_3$-based systems to $ZT \approx 1.5$.[4–11] Achieving a $ZT \geq 2$ in such inorganic semiconductors remains a research target, as it would enable conversion efficiencies of ~10% (e.g., at $T_c$ = 300 K and $T_h$ = 550 K) and make TEGs more viable for large-scale energy applications.[12–16]

## BACKGROUND

Although TEGs produce electricity without direct GHG emissions, their overall sustainability remains uncertain once the energy- and resource-intensive nature of their manufacturing is considered. Processes such as rare metal extraction, element refining, alloy synthesis, device fabrication, and disposal can significantly offset the environmental benefits of waste-heat recovery. With commercial devices operating at <5% efficiency, energy payback times (EPBTs) may extend well beyond practical lifetimes. Despite major advances in TE materials research, sustainability assessments of TEGs have lagged, and the literature still lacks a comprehensive account of their life-cycle environmental profile.

Recent studies have begun addressing this gap by examining the life-cycle GHG emissions or techno-economics of TEGs in specific contexts, such as automobile exhaust recovery,[17,18] hybrid integration with photovoltaic (PV) cells,[19–22] and phase-change material (PCM)-based refrigeration.[23] The first set of studies explored whether TEG deployment in automobiles (where large temperature gradients exist) can reduce life-cycle $CO_2$ emissions. The second examined the potential of TEGs to improve the EPBT of PV systems and assessed whether their integration is economically viable. The third compared the GHG emissions of PCM-based refrigerators with magnetic ones.

Please cite this article in press as: Pakdel and Reilly, Life-cycle assessment of carbon footprint and energy intensity of thermoelectric generator production for near-room-temperature applications, Device (2026), https://doi.org/10.1016/j.device.2026.101085



These targeted studies highlight important application-specific insights, but they do not provide a comprehensive production-stage baseline for TEGs themselves, nor do they resolve module bill of materials, route-specific manufacturing energy, or device-level payback metrics.

This study addresses that gap by presenting a process-resolved, cradle-to-gate life cycle assessment (LCA) of $Bi_2Te_3$-based TEGs (the most widely used TE devices) by measuring their environmental impact from raw material extraction (cradle) to manufacturing and factory exit (gate), as illustrated in Figure 1B. The work quantifies cumulative energy demand (CED) for TE materials preparation and TEG production, compares two well-known manufacturing routes (i.e., crystal growth vs. powder metallurgy), and includes key non-TE components (e.g., Cu interconnects and leads, Ni contact layers, $Al_2O_3$ plates, epoxy, and polyvinyl chloride [PVC]). The production inventory is then coupled to device performance to estimate EPBT as a function of temperature gradient and duty-cycle assumptions. The production-stage carbon footprint is also quantified by life-cycle stage, and the minimum operating time needed for a TEG to offset manufacturing emissions is assessed. Finally, the environmental performance of a low-cost commercial TEG is compared with that of an advanced research-grade module. Figure 1C provides the research roadmap for a cradle-to-gate LCA of TEGs, with full definitions in the results and discussion. These results provide a quantitative baseline for judging whether TEGs can be environmentally viable for near-room-temperature applications and where design and process changes deliver the largest gains. As future work, the present baseline can be extended with use-phase variability and end-of-life (EoL) scenarios (collection, recovery yields, and allocation choices) to complete a full cradle-to-cradle life-cycle picture.

This study was conducted in two main phases: data collection and system definition and life-cycle modeling and impact assessment. In the first phase, a literature review was performed to gather relevant data on the production and performance of a unit $Bi_2Te_3$-based TEG. Sources included peer-reviewed journal articles, governmental reports, industrial documents, and technical specification sheets from TEG manufacturers. They were chosen based on direct relevance to $Bi_2Te_3$ TEG manufacturing/performance, availability of extractable quantitative parameters, and credibility/traceability (peer-reviewed or authoritative technical sources). In the second phase, the collected data were used to prepare a life-cycle model of the TEG system. The model was developed and analyzed using GaBi software (Sphera, USA), an LCA platform.

As detailed in the methods section, two types of $Bi_2Te_3$-based TEGs were investigated: typical low-cost commercial TEGs (hereafter referred to as type A) and advanced research-grade TEGs (hereafter referred to as type B). Type-A devices consisted of p-type $Bi_2Te_3$ legs doped with Sb (~1 wt %) and n-type $Bi_2Te_3$ legs doped with Se (~1 wt %). These TEGs were assumed to exhibit a $ZT_{avg} \approx 1$, representing potential best-case performance scenarios under optimized conditions. The TE legs in type-B devices were made of p-type $Bi_{0.5}Sb_{1.5}Te_3$ and n-type $Bi_2Te_{2.7}Se_{0.3}$. The TE performance of these materials can be enhanced through nanostructuring, incorporation of secondary nanoparticle phases, grain boundary engineering, and band or defect engineering strategies.[24–39] A $ZT_{avg} \approx 1.5$ was assumed for type-B devices, representing an optimistic yet literature-supported performance benchmark. Finally, it was assessed whether the environmental costs of elemental extraction and energy-intensive material synthesis and module processing may undermine the TEG's core function as a renewable energy technology.

## RESULTS AND DISCUSSION

### CED of TEG module production

The total energy required to manufacture one TEG unit, using either the crystal growth or powder metallurgy route, is shown in Figure 2A, with calculation details in Note S8. The results were divided into four categories: (1) extraction and refining of TE elements, (2) TE material synthesis, (3) non-TE material extraction and processing, and (4) transportation. This breakdown provides insights into the relative contributions of each process to the total environmental footprint of the device. Among these stages, TE material synthesis accounted for the largest share of energy demand, but the extraction and refining of TE elements contributed less energy per unit of TEG. The crystal growth route was significantly more energy intensive, consuming on average 219% more energy than the powder metallurgy route. As a result, the total input energy for fabricating type-A and type-B TEGs via the Bridgman method was 67% and 72% higher, respectively, compared to their counterparts produced via powder metallurgy. Contributions from transportation and non-TE materials were negligible in both cases.

This energy discrepancy had a direct impact on the EPBT, as shown in Figure 2B. TEGs manufactured using the crystal growth method required approximately 215% longer to recover their embodied energy (at $\Delta T = 30^{\circ}C$) compared to modules produced via powder metallurgy. In addition, type-B TEGs demonstrated a shorter EPBT, approximately 40% that of type-A TEGs, which highlights the role of advanced TE materials in improving the energy sustainability of TEGs.

Figure 2C illustrates the sensitivity of EPBT to varying temperature gradients under continuous operation. At low $\Delta T$ values (e.g., 10°C), the EPBT spanned from 24 to 74 years, suggesting that TEGs operating under such conditions were unlikely to offset their manufacturing energy within a practical lifetime. In contrast, at high $\Delta T$ values (e.g., 70°C), the EPBT plummeted to 0.5–1.5 years, making TEGs a favorable energy-conversion technology. Further details on the EPBT calculation methodology and assumptions are provided in Note S9. It should be noted that if TEGs operate for fewer than 24 h/day, a correction factor should be applied to the EPBT values in Figure 2C, as will be discussed in the sensitivity analysis.

### Global warming potential of the TEG life cycle

Global warming potential (GWP) is a standard metric used to quantify the relative climate impact of GHGs. It is expressed in units of kg $CO_2$ equivalent (kg $CO_2$-equiv) and compares the heat absorbed by a given mass of a gas to that absorbed by the same mass of $CO_2$, whose GWP is set to 1. In the TEG life cycle, electricity use represents the major source of GHG emissions. In this study, China's electrical grid was chosen as the energy source for the extraction, synthesis, and processing

Please cite this article in press as: Pakdel and Reilly, Life-cycle assessment of carbon footprint and energy intensity of thermoelectric generator production for near-room-temperature applications, Device (2026), https://doi.org/10.1016/j.device.2026.101085



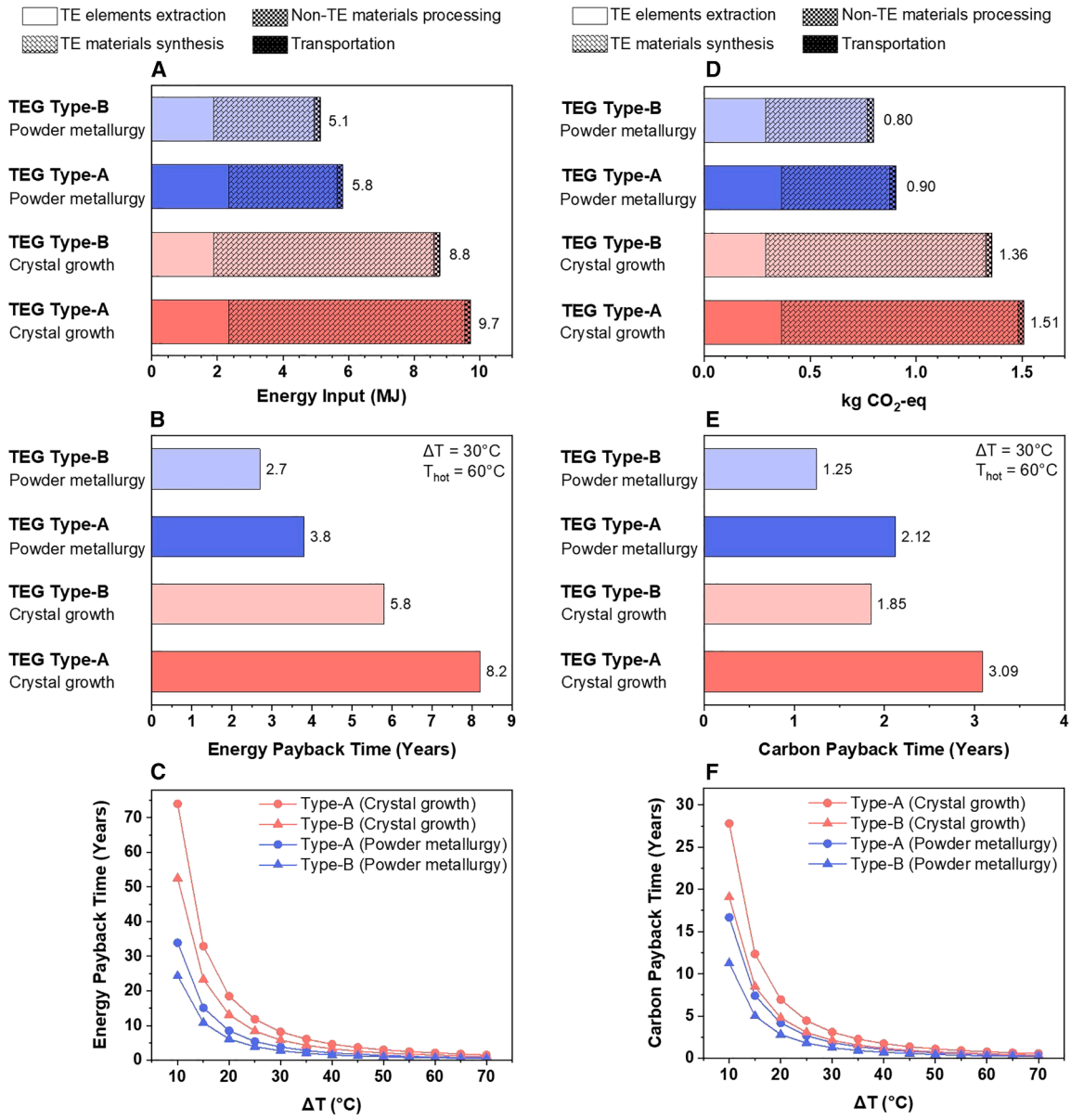


**Figure 2. Energy, carbon, and payback metrics of TEG production**

(A–C) Comparing the energy input and output for all TEGs in terms of (A) CED required for manufacturing, (B) EPBT based on the initial assumption of $T_{cold}$ = 30°C and $\Delta T$ = 30°C, (C) EPBT for a range of temperature gradients between $\Delta T$ = 10°C and 70°C (and $T_{cold}$ = 30°C in all cases).

(D–F) Comparing the relative climate impact for all TEGs in terms of (D) GWP for different stages of TEG production, (E) CPBT based on the initial assumption of $T_{cold}$ = 30°C and $\Delta T$ = 30°C, and (F) CPBT for a range of temperature gradients between $\Delta T$ = 10°C and 70°C (and $T_{cold}$ = 30°C in all cases).

stages, as it represents the dominant location of current TE material supply chains (further details in Note S4). However, the sensitivity analysis section discusses how results could be affected by substituting lower-carbon grids in the European Union or the United States. Based on official reports by the Ministry of Ecology and Environment of China (MEE), an average emission factor (AEF) of 0.5568 kg $CO_2$/kWh (0.1547 kg $CO_2$/MJ) was applied.[40] In contrast, many commercial LCA databases, such as GaBi and CES EduPack, report substantially lower emission factors (≤0.07 kg $CO_2$/MJ), which underestimate the role of coal in the Chinese electricity mix. Transportation emissions were also considered, based on IPCC data indicating that a 20-ton diesel truck typically consumes ~2.67 kg $CO_2$/L of fuel.[41] With an assumed average fuel economy of ~25 L/100 km,[42] this corresponds to ~0.6408 kg $CO_2$/km.

Figure 2D shows the contribution of each life-cycle stage (TE element extraction/refining, TE material synthesis, non-TE material production, and transportation) to the total GWP of type-A and type-B TEGs. Results indicate that the TE material synthesis stage dominated the GWP profile, particularly for the crystal

Please cite this article in press as: Pakdel and Reilly, Life-cycle assessment of carbon footprint and energy intensity of thermoelectric generator production for near-room-temperature applications, Device (2026), https://doi.org/10.1016/j.device.2026.101085



growth route, where prolonged high-temperature furnace operation resulted in higher emissions compared to powder metallurgy. For instance, the crystal growth synthesis step accounted for approximately 74% and 76% of the total GWP in type-A and type-B TEGs, respectively, while the powder metallurgy synthesis contribution to the total GWP in type-A and type-B TEGs was 56% and 60%, respectively. Non-TE components (Cu, Ni, $Al_2O_3$, epoxy, and PVC) and transportation had negligible effects on the overall GWP, together representing less than 3% of the total. Overall, switching from crystal growth to powder metallurgy reduced the total GWP of TEG production by ~40%, consistent with the CED results. These findings underscore the importance of synthesis route optimization in reducing the climate impact of TE module manufacturing. Further details on the GWP calculation methodology are provided in Note S10.

Another concept related to GWP is the carbon payback time (CPBT), which complements the EPBT by quantifying how long a TEG must operate to offset the GHG emissions generated during its production. Based on the manufacturing footprints in Figure 2D and assuming continuous operation under $\Delta T$ = 30°C, the CPBTs of all TEGs are presented in Figure 2E and detailed in Note S11. The results show that type-A and type-B TEGs produced via crystal growth needed approximately 3.1 and 2.1 years, respectively, to offset their embodied emissions. In contrast, type-A and type-B modules fabricated via powder metallurgy required only 1.9 and 1.3 years, respectively. These values reinforce the conclusion that powder metallurgy was the more sustainable synthesis route, both in terms of energy and carbon emissions. Moreover, the shorter CPBTs of type-B modules highlight the benefits of advanced chemical compositions with improved efficiency.

The sensitivity of CPBT to operating conditions is illustrated in Figure 2F. At low $\Delta T$ values (e.g., 10°C), CPBT ranged from ~11 to 28 years across the four TEG types, suggesting that under modest gradients, the modules were less likely to offset their manufacturing-related $CO_2$ emissions within a practical lifespan. In contrast, at higher $\Delta T$ values (e.g., 70°C), the CPBT rapidly decreased to only 0.2–0.6 years, showing that TEGs could achieve net climate benefits when deployed in high-thermal-gradient environments. As with EPBT, CPBT values scale linearly with operational hours: if TEGs were used for fewer than 24 h per day, the corresponding CPBT values must be adjusted proportionally upward. Overall, these results emphasize that both the synthesis route (i.e., crystal growth vs. powder metallurgy) and the operational conditions (i.e., temperature gradient and duty cycle) are critical in determining whether TEGs are environmentally favorable from a carbon emissions perspective.

Another important factor influencing the GWP results is the type of electricity used in the production process. Today, the Chinese electricity grid mix remains heavily reliant on coal, which accounts for approximately 53%–58% of total generation, followed by hydropower (13%–15%), wind power (10%–12%), solar power (5%–7%), nuclear power (4%–5%), natural gas (3%–6%), and biomass (1%–2%).[43–45] To assess the sensitivity of the results to the electricity source, a scenario analysis was performed. A type-A TEG produced via the crystal growth route was selected for this comparison, as it required the highest input energy and produced the largest GHG emissions in the baseline case. As shown in Figure 3A, sourcing electricity entirely from coal increased the GWP by 60% compared to the average Chinese grid mix. In contrast, using renewable or low-carbon sources (e.g., wind or hydropower) reduced the GWP by around 95%, while solar power and biomass would also achieve reductions of ≥85%. These results highlight that the carbon intensity of the electricity mix is a decisive factor in determining the overall climate footprint of TEGs. Reducing dependence on fossil fuels and expanding the share of renewables in electricity supply could substantially lower the GWP of TEG production, thereby improving the overall sustainability of TE devices. A similar comparison for all TEG types is provided in Figure 3B. Further details on the GWP calculation methodology are provided in Note S12.

## Terrestrial acidification, freshwater eutrophication, and human toxicity impact

In addition to GHG emissions, the life cycle of TEGs can also contribute to other environmental impact categories, such as terrestrial acidification potential (AP), freshwater eutrophication potential (EP), and human toxicity potential (HTP). AP (kg $SO_2$-equiv) reflects emissions of acidifying substances such as $SO_2$, $NO_x$, and $NH_3$, which lead to acid rain and soil acidification. EP (kg P-equiv) measures the nutrient enrichment of freshwater ecosystems, which can trigger algal blooms and deplete dissolved oxygen. HTP (CTUh) estimates the potential risk to human health from toxic substance exposure, expressed as the probability of disease cases per kilogram of product.[46]

To quantify non-climate impacts for the TE elements, the cradle-to-gate characterization factors compiled by Nuss and Eckelman[47] were used, implemented in SimaPro and ecoinvent foreground/background inventories. For each module, impacts were calculated by simple mass weighting of element-level factors ($impact_{module} = \sum_i m_i \times CF_i$, where $m_i$ is the mass of element $i$ in the module and $CF_i$ is the characterization factor (AP, EP, or HTP) per kg of that element. Figure 4 shows representative AP, EP, and HTP values for the TE elements used in type-A and type-B TEGs, based on the mass data from the life-cycle inventory (LCI). Table 1 presents the converted values as contribution percentages. For type-A TEGs, Te accounts for 85.6% of AP, with Bi (14.2%) forming a meaningful second tier, but Sb and Se are each <0.1%. For type-B TEGs, Te remains dominant in AP (88.2%), while Bi (9.5%) is the next contributor, and Sb rises to 2% due to its higher loading. In EP, Te is overwhelming in both modules (97.2% for type A and 92% for type B). Sb becomes the second contributor in type B (~6.3%), reflecting the combination of its larger mass fraction and a relatively high EP factor. Bi and Se are each ≤0.1%. For HTP, Te again dominates (98.7% for type A and 93.6% for type B), with 5.6% of Sb in type B and ≤1% of Bi/Se. Further details on the impact calculation methodology are provided in Note S13.

While Te is the leading driver in all three categories (AP, EP, and HTP), Bi and Sb have a notable second rank. Se, on the other hand, had a minor contribution for both TEG types, reflecting its low mass fractions and comparatively smaller environmental impact factors. Synthesis, assembly steps, and non-TE components were not included here, and adding them would not change the ranking but would redistribute shares. For example, Ni interlayers and Cu interconnects tend to increase AP via upstream

Please cite this article in press as: Pakdel and Reilly, Life-cycle assessment of carbon footprint and energy intensity of thermoelectric generator production for near-room-temperature applications, Device (2026), https://doi.org/10.1016/j.device.2026.101085



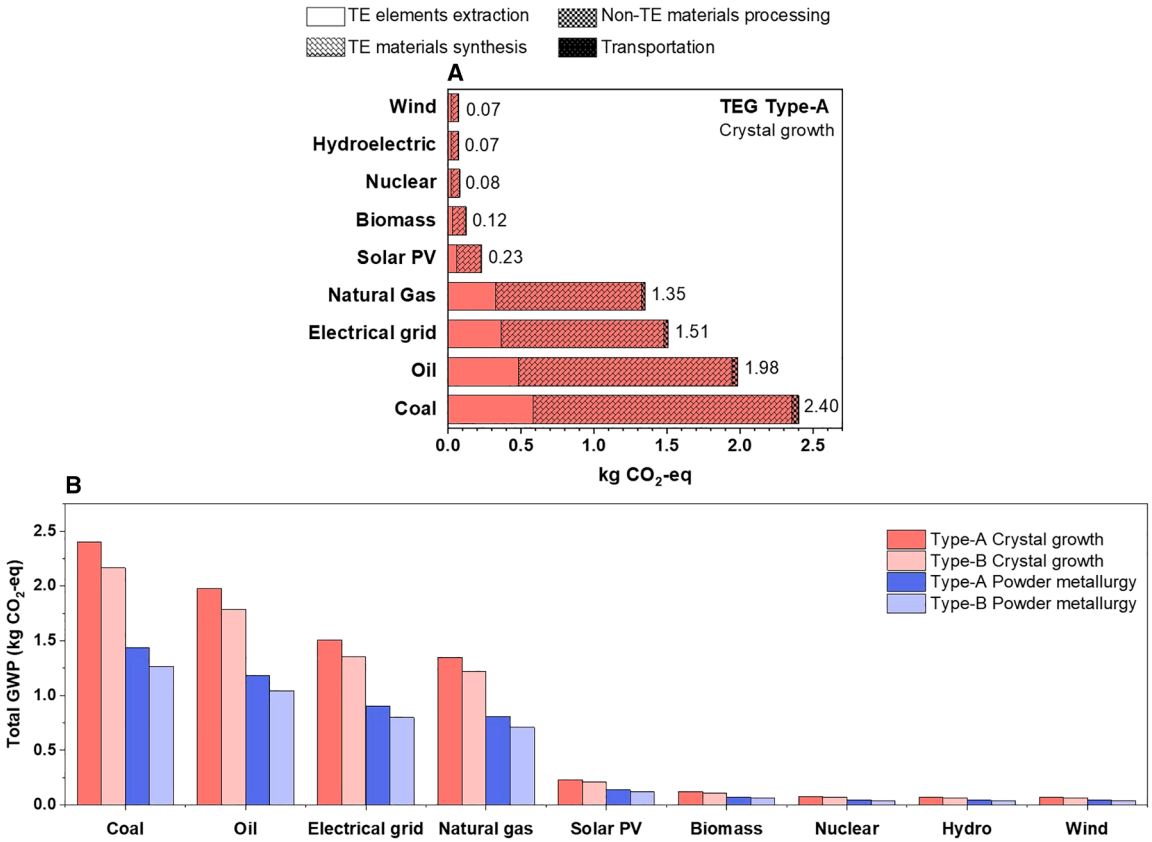


**Figure 3. Sensitivity of TEG carbon footprint to electricity source**

(A) Energy source sensitivity analysis of the GWP in different stages of TEG production for type-A TEG manufactured via the crystal growth route.

(B) Sensitivity analysis of the total manufacturing GWP in all TEGs with respect to the electricity source.

$SO_2$/$NO_x$, slightly decreasing the fractional contributions of Te. Likewise, including synthesis electricity increases AP/EP totals (especially for crystal growth), yet the qualitative ordering remains unchanged (powder metallurgy < crystal growth; type B < type A).

From a mitigation standpoint, multiple strategies should be considered: (1) improving TE material efficiency and optimizing leg geometry in TEGs to deliver more watts per gram of TE materials, (2) prioritizing responsible sourcing from smelters with effective flue-gas desulfurization and wastewater treatment to curb acidification and eutrophication drivers, (3) implementing closed-loop recovery of Te/Sb/Bi after production steps and from EoL modules, and (4) where feasible, using renewable low-carbon electricity for synthesis processes.

## Supply concentration and sustainability implications

The LCI results (Note S4) highlighted that several key TE elements (e.g., Te, Sb, and Bi) have concentrated global supply chains. For instance, over 90% of the world's Sb is produced in China, Russia, and Tajikistan, while China also dominates global production of Bi and Te.[48,49] Such geographic concentration could create structural vulnerabilities for the TE sector by exposing it to supply chain disruptions, price volatility, and geopolitical risks.[48] At the same time, it concentrates environmental and social burdens (e.g., pollution, labor conditions, and safety risks) within a small number of regions, raising concerns about both resilience and fairness in the TE value chain.

This issue is not unique to TEGs and is shared with other renewable energy technologies. For example, 92% of rare earths for wind turbines are produced in China, the United States, and Canada; 86% of Co for batteries is produced in Congo (Kinshasa), Indonesia, and Russia; 74% of Li for batteries is produced in Australia, Chile, and China; and 92% of high-purity silicon for PV is produced in China, Brazil, and Norway.[49] This means that while TEGs are not exceptional in their dependence on concentrated supply, their reliance on by-products such as Te makes them especially vulnerable, as production volumes are tied to demand in other sectors (e.g., Cu). Thus, unlike bulk metals (e.g., Fe and Al), where supply can be expanded relatively easily, scaling TEG deployment is constrained by these upstream dependencies. These dynamics highlight the importance of risk mitigation strategies, including diversifying and certifying sources, optimizing co-product recovery at copper/lead refineries, closed-loop recovery from manufacturing scrap and EoL modules, and exploring material substitution.

## Sensitivity analysis

The robustness of an LCA depends on the quality and representativeness of the underlying data. In the present assessment,

Please cite this article in press as: Pakdel and Reilly, Life-cycle assessment of carbon footprint and energy intensity of thermoelectric generator production for near-room-temperature applications, Device (2026), https://doi.org/10.1016/j.device.2026.101085





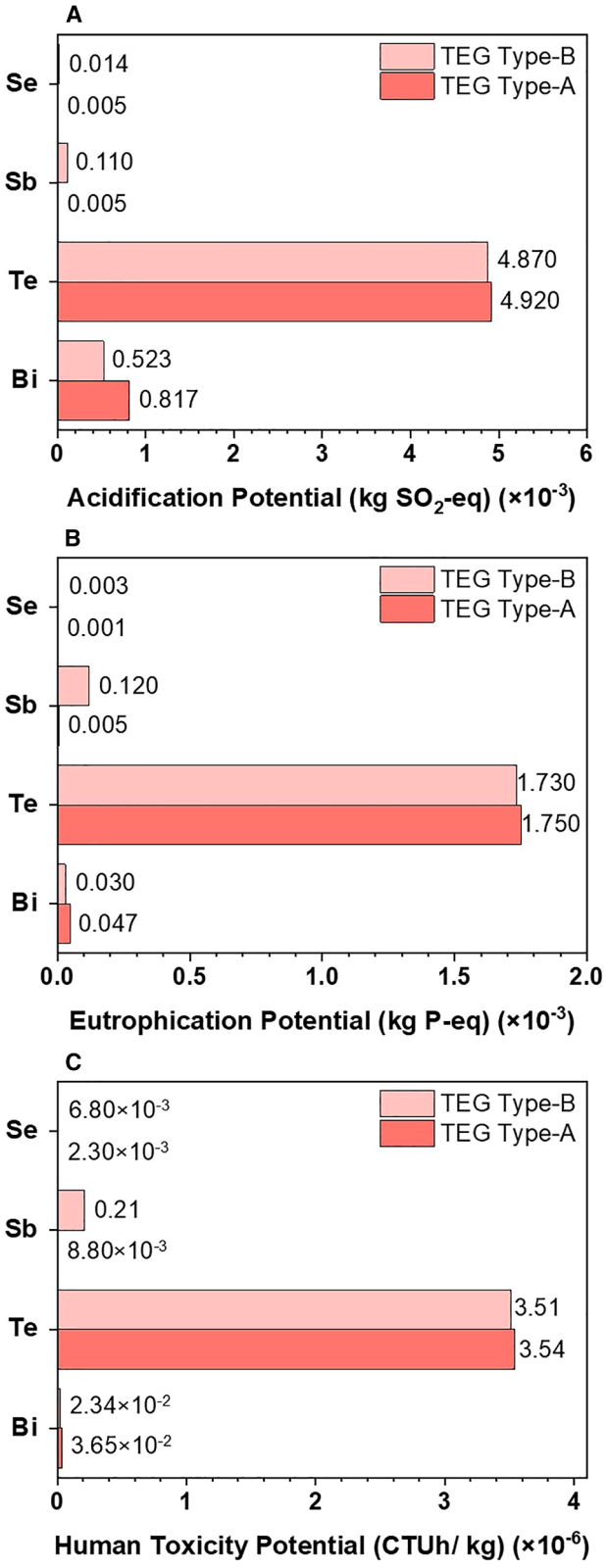


**Figure 4. Non-climate environmental impacts of TE elements**

Comparing the environmental impact factor of TE elements in TEGs in terms of (A) terrestrial acidification potential, (B) freshwater eutrophication potential, and (C) human toxicity potential.

primary data were used wherever possible, particularly for process-level energy consumption (e.g., furnace melting, spark plasma sintering [SPS], and ball milling). These values were derived from manufacturer specifications and cross-checked against reported literature data and the GaBi database. Nevertheless, the energy requirements of synthesis routes remain a potential source of variability. In this study, machine power ratings and process durations were based on large laboratory (or pilot-scale) equipment representative of start-up or pre-commercial practice rather than small benchtop tools or fully industrial continuous lines. No attempt was made to scale these data to mass production; instead, nameplate power and typical duty cycles from vendor documentation were used to reflect realistic but conservative operating envelopes. Therefore, the estimated energy demand should be considered an upper bound for a given module design. At an industrial scale, higher tray loading, multi-cavity tooling, improved thermal integration, and better uptime can reduce specific electricity per kilogram. Therefore, the absolute EPBT and CPBT may be shorter relative to the figures reported here.

To demonstrate scalability, a parametric batch-yield factor (β) was defined, capturing the ratio of "actual run mass" to the baseline lab run mass (i.e., how much material is consolidated per crystal-growth/sintering cycle). Because a given cycle's electricity draw is largely time driven rather than mass proportional (within equipment capacity), per-kg energy decreases approximately as 1/β. This was applied to the synthesis portion of CED only (other contributions are unaffected), and changes to EPBT/CPBT were calculated using the equations here, as demonstrated in Table 2:

$$CED_{\beta} = \left(CED_{total} - CED_{synthesis}\right) + \frac{CED_{synthesis}}{\beta}, \quad \text{(Equation 1)}$$

**Table 1. Comparing contributions from thermoelectric elements to non-climate environmental impacts in TEGs**

| | Environmental impacts | | |
|---|---|---|---|
| Element | Acidification potential contribution | Eutrophication potential contribution | Human toxicity potential contribution |
| TEG type A | | | |
| Bi | 14.2% | 2.6% | 1.0% |
| Te | 85.6% | 97.2% | 98.7% |
| Sb | 0.1% | 0.3% | 0.3% |
| Se | 0.1% | <0.1% | <0.1% |
| TEG type B | | | |
| Bi | 9.5% | 1.6% | 0.6% |
| Te | 88.2% | 92.0% | 93.6% |
| Sb | 2.0% | 6.3% | 5.6% |
| Se | 0.3% | 0.1% | 0.2% |

Please cite this article in press as: Pakdel and Reilly, Life-cycle assessment of carbon footprint and energy intensity of thermoelectric generator production for near-room-temperature applications, Device (2026), https://doi.org/10.1016/j.device.2026.101085



**Table 2. Sensitivity analysis of the cumulative energy demand and energy payback time under batch-yield scaling (β)**

| TEG | Route | CED (MJ), β = 1 | CED (MJ), β = 2 | CED (MJ), β = 5 | CED (MJ), β = 10 |
|---|---|---|---|---|---|
| Type A | crystal growth | 9.735 | 6.139 | 3.981 | 3.261 |
| Type B | crystal growth | 8.792 | 5.429 | 3.411 | 2.739 |
| Type A | powder metallurgy | 5.827 | 4.185 | 3.199 | 2.871 |
| Type B | powder metallurgy | 5.137 | 3.602 | 2.680 | 2.373 |
| TEG | Route | EPBT (y), β = 1 | EPBT (y), β = 2 | EPBT (y), β = 5 | EPBT (y), β = 10 |
| Type A | crystal growth | 8.2 | 5.2 | 3.4 | 2.7 |
| Type B | crystal growth | 5.8 | 3.6 | 2.3 | 1.8 |
| Type A | powder metallurgy | 3.8 | 2.7 | 2.1 | 1.9 |
| Type B | powder metallurgy | 2.7 | 1.9 | 1.4 | 1.2 |
| TEG | Route | CPBT (y), β = 1 | CPBT (y), β = 2 | CPBT (y), β = 5 | CPBT (y), β = 10 |
| Type A | crystal growth | 3.1 | 2.0 | 1.3 | 1.0 |
| Type B | crystal growth | 2.1 | 1.3 | 0.8 | 0.7 |
| Type A | powder metallurgy | 1.9 | 1.4 | 1.0 | 0.9 |
| Type B | powder metallurgy | 1.3 | 0.9 | 0.7 | 0.6 |

| TEG | Route | China (kg $CO_2$-equiv/TEG) | United States (kg $CO_2$-equiv/TEG) | EU-27 (kg $CO_2$-equiv/TEG) |
|---|---|---|---|---|
| Type A | crystal growth | 1.506 | 1.093 | 0.877 |
| Type B | crystal growth | 1.355 | 0.971 | 0.770 |
| Type A | powder metallurgy | 0.903 | 0.714 | 0.615 |
| Type B | powder metallurgy | 0.798 | 0.621 | 0.528 |

Sensitivity analysis of the effect of regional electricity mixes on TEG manufacturing GWP (the type-A TEG was manufactured via the crystal growth route, complementary to the analysis presented in Figure 4)

$$EPBT_{\beta} = EPBT_{baseline} \times \frac{CED_{\beta}}{CED_{baseline}}, \text{ and} \quad \text{(Equation 2)}$$

$$CPBT_{\beta} = CPBT_{baseline} \times \frac{CED_{\beta}}{CED_{baseline}}. \quad \text{(Equation 3)}$$

Another assumption concerns the electricity emission factors for China. Because electricity supply is the dominant factor influencing the GWP results, the baseline model assuming an average Chinese electricity grid was compared with alternative electricity mixes, including fossil based and renewable, as shown in Figure 4. It is evident that relocating extraction, processing, and synthesis to regions with cleaner electricity grids would lower the GWP.

As an example, geographic variability was tested by recalculating GWP using representative average grid $CO_2$ intensities for the United States (≈0.35 kg $CO_2$ $kWh^{-1}$) and the European Union (≈0.24 kg $CO_2$ $kWh^{-1}$), alongside the baseline China factor (0.5568 kg $CO_2$ $kWh^{-1}$). As summarized in Table 2, total per-TEG GWP decreases by ∼21%–28% under the United States' average grid and by ∼32%–44% under the EU-27 average, across all four module types. The ranking, however, remains unchanged (powder metallurgy < crystal growth; type B < type A). These geographic results complement the technology-specific scenarios in Figure 4.

The interpretation of EPBT, CPBT, and related energy and carbon indicators is also sensitive to assumptions about TEG efficiency. In this study, power output values were derived from representative commercial data under an assumed $T_{cold}$ = 30°C and $\Delta T$ = 30°C. However, real-world operation may involve lower or higher temperatures and gradients, seasonal variations, or intermittent duty cycles. These factors should be accounted for when estimating the EPBT and CPBT in specific applications, as briefly illustrated in Figures 2C and 2F.

The reported EPBTs and CPBTs assumed continuous operation under a constant temperature gradient. However, as real-world factors such as thermal cycling, aging, and efficiency degradation can lead to underestimation of these parameters, a sensitivity analysis was performed to account jointly for duty cycle ($D$) and annual performance degradation rate ($R$). If $t_0$ is the baseline payback time (years) at continuous operation ($D$ = 1) with no performance decay, then for a duty cycle $0 < D < 1$, the adjusted payback time $t$ is $t = \frac{t_0}{D}$. If an annual performance degradation rate $R$ (fraction/year) is also included, the adjusted payback time $t$ can be calculated as $t = \frac{\ln(1 - Rt_0/D)}{\ln(1-R)}$. If $\frac{Rt_0}{D} \geq 1$, payback becomes unattainable, and the device cannot earn back its embodied energy or emissions. Since both the EPBT and CPBT scale with delivered energy, the same adjustment applies to both metrics.

Table 3 shows the sensitivity calculations for payback time (years) at duty cycles of 25%, 50%, 75%, and 100% and annual degradation rates of 0%, 1%, 2%, 5%, and 10%, as examples. Overall, the sensitivity analysis highlights that conclusions about sustainability hinge on how and where TEGs operate. Modules utilized at low duty cycles in harsh environments (high $R$) may not achieve payback within practical lifetimes, whereas high duty cycles with modest degradation reliably do, especially for type-B modules made via powder metallurgy.

The non-climate impact results are strongly influenced by the choice of assumed inventory or sourcing pathway of TE materials and region-specific impact factors. For instance, the

Please cite this article in press as: Pakdel and Reilly, Life-cycle assessment of carbon footprint and energy intensity of thermoelectric generator production for near-room-temperature applications, Device (2026), https://doi.org/10.1016/j.device.2026.101085





**Table 3. Sensitivity analysis of the energy payback time and carbon payback time in all TEGs at different duty cycles (D) and annual degradation rates (R)**

| | *R* | | | | |
|---|---|---|---|---|---|
| *D* | 0% | 1% | 2% | 5% | 10% |
| EPBT: type A, crystal growth | | | | | |
| 100% | 8.2 | 8.5 | 8.9 | 10.3 | 16.3 |
| 75% | 10.9 | 11.5 | 12.2 | 15.4 | N/A |
| 50% | 16.4 | 17.8 | 19.7 | 33.4 | N/A |
| 25% | 32.8 | 39.6 | 52.8 | N/A | N/A |
| EPBT: type B, crystal growth | | | | | |
| 100% | 5.8 | 6.0 | 6.1 | 6.7 | 8.2 |
| 75% | 7.7 | 8.0 | 8.3 | 9.5 | 14.1 |
| 50% | 11.6 | 12.3 | 13.1 | 16.9 | N/A |
| 25% | 23.2 | 26.3 | 30.9 | N/A | N/A |
| EPBT: type A, powder metallurgy | | | | | |
| 100% | 3.8 | 3.9 | 3.9 | 4.1 | 4.5 |
| 75% | 5.1 | 5.2 | 5.3 | 5.7 | 6.7 |
| 50% | 7.6 | 7.9 | 8.2 | 9.3 | 13.6 |
| 25% | 15.2 | 16.4 | 17.9 | 27.8 | N/A |
| EPBT: type B, powder metallurgy | | | | | |
| 100% | 2.7 | 2.7 | 2.8 | 2.8 | 3.0 |
| 75% | 3.6 | 3.7 | 3.7 | 3.9 | 4.2 |
| 50% | 5.4 | 5.5 | 5.7 | 6.1 | 7.4 |
| 25% | 10.8 | 11.4 | 12.1 | 15.1 | N/A |
| CPBT: type A, crystal growth | | | | | |
| 100% | 3.1 | 3.1 | 3.2 | 3.3 | 3.5 |
| 75% | 4.1 | 4.2 | 4.3 | 4.5 | 5.1 |
| 50% | 6.2 | 6.4 | 6.6 | 7.2 | 9.2 |
| 25% | 12.4 | 13.2 | 14.1 | 18.9 | N/A |
| CPBT: type B, crystal growth | | | | | |
| 100% | 2.1 | 2.1 | 2.1 | 2.2 | 2.2 |
| 75% | 2.8 | 2.8 | 2.9 | 2.9 | 3.1 |
| 50% | 4.2 | 4.3 | 4.3 | 4.6 | 5.2 |
| 25% | 8.4 | 8.7 | 9.1 | 10.6 | 17.4 |
| CPBT: type A, powder metallurgy | | | | | |
| 100% | 1.9 | 1.9 | 1.9 | 2.0 | 2.0 |
| 75% | 2.5 | 2.6 | 2.6 | 2.6 | 2.8 |
| 50% | 3.8 | 3.9 | 3.9 | 4.1 | 4.5 |
| 25% | 7.6 | 7.9 | 8.2 | 9.3 | 13.6 |
| CPBT: type B, powder metallurgy | | | | | |
| 100% | 1.3 | 1.3 | 1.3 | 1.3 | 1.3 |
| 75% | 1.7 | 1.7 | 1.8 | 1.8 | 1.8 |
| 50% | 2.6 | 2.6 | 2.6 | 2.7 | 2.9 |
| 25% | 5.2 | 5.3 | 5.4 | 5.9 | 7.0 |

*D*, duty cycle; *R*, annual degradation rate.

impacts on acidification and eutrophication in this study were based on the ReCiPe midpoint method (version 1.08/H) for the globe, where the LCI data is translated into 18 mid-level environmental impact categories based on the Hierarchist (H) perspective.[50] However, alternative regionalized characterization factors or process-specific inventories could shift absolute impact magnitudes without altering the relative contribution trends discussed here.

While we report baseline CED/GWP for TEG production through crystal growth and powder metallurgy routes, there are other engineering levers that can further reduce the impacts. For instance, for crystal growth, improved hot-cold zone insulation and interface control can reduce heat leakage and energy waste.[51,52] Other synthesis techniques, such as alternative/assisted heating (e.g., microwave synthesis and flash/field-assisted sintering), can shorten thermal cycles by orders of magnitude relative to conventional furnaces.[53,54] Likewise, optimization of SPS parameters (pulse schedule, pressure, and die geometry) can also influence energy consumed per batch. In addition, generic process-heating studies support heat recovery and excess air control as practical measures that can deliver considerable efficiency gains.[55]

## CONCLUSION AND OUTLOOK

We provided an LCA of $Bi_2Te_3$-based TEGs for near-room-temperature thermal energy conversion. We compared two TE material composition scenarios in TEGs: type A, consisting of typical commercial p- and n-type $Bi_2Te_3$, and type B, made of more recent and advanced p-type $(Bi, Sb)_2Te_3$ and n-type $Bi_2(Te, Se)_3$. We evaluated two synthesis routes for TE materials, i.e., conventional crystal growth and powder metallurgy. The analysis covered CED, EPBT, GWP, and selected non-climate impact categories (acidification, eutrophication, and human toxicity).

The results demonstrated that TE material synthesis was the hotspot and that it dominated the life-cycle energy and climate impacts of TEGs. The TE element extraction/refining and the non-TE component (Ni, Cu, $Al_2O_3$, epoxy, and PVC) preparations contributed only marginally, and transportation's contribution was negligible. Crystal growth was found to be more than twice more energy intensive than powder metallurgy, leading to EPBTs that were ~215% longer under identical operating conditions. For example, at $\Delta T$ = 30°C, type-A and type-B modules produced by crystal growth required 67% and 72% more energy, respectively, than their powder metallurgy counterparts. At low temperature gradients (e.g., $\Delta T$ = 10°C), EPBTs and CPBTs ranged between 2 and 7 decades and 1 and 3 decades, respectively, most likely exceeding realistic TEG lifetimes. However, under higher gradients (e.g., $\Delta T$ = 70°C), the EPBT and CPBT were reduced to 0.5–1.5 and 0.2–0.6 years, respectively, suggesting that these TEGs can be more environmentally competitive in mid- and high-grade waste-heat recovery scenarios.

With respect to climate impacts, the total GWP per TEG was estimated in the range of 0.80–1.51 kg $CO_2$-equiv, depending on module type and synthesis route. Synthesis represented the dominant contributor, accounting for up to 74%–76% of the total GWP in conventional modules manufactured through the crystal growth route. The choice of electricity source was shown to be decisive. If combustion-based electricity generation were exclusively used, emission levels could increase by ~60% relative to the grid average, while renewable electricity (e.g., hydro, wind, etc.) could cut emissions by over 90%. This highlights the

Please cite this article in press as: Pakdel and Reilly, Life-cycle assessment of carbon footprint and energy intensity of thermoelectric generator production for near-room-temperature applications, Device (2026), https://doi.org/10.1016/j.device.2026.101085



importance of coupling TEG development with decarbonized electricity grids to ensure their sustainability.

Beyond climate change, the analysis of other environmental categories in relation to the extraction/refining of TE elements indicated that among them, tellurium was the primary driver of acidification (up to 0.0049 g $SO_2$-equiv per TEG), eutrophication (up to 0.0018 g P-equiv per TEG), and human toxicity (up to $3.5 \times 10^{-6}$ CTUh per TEG) impacts, due to its high characterization factors and relatively large mass fractions in the TE legs. Bismuth and antimony contributed secondarily, while selenium's contribution was negligible. These results imply that tellurium recovery and recycling strategies are essential to mitigate the broader environmental burdens of TEG production.

Taken together, the results indicate the following high-leverage pathways to improve the sustainability of $Bi_2Te_3$-based TEGs. Switching from conventional crystal growth to powder metallurgy and tightening process control (better refractory/insulation, load matching, heat recovery, and excess air control) can lower CED and GWP by ~40% at the module level, with further gains from higher batch utilization and recent fast-sintering/SPS variants. Electricity decarbonization during extraction and synthesis can cut manufacturing GWP by up to 95%, making location and procurement policy central to impact reduction. Material strategies that reduce TE intensity, raise the watts per gram of the TE material, and build closed-loop recovery (production scrap and, in the future, EoL modules) can curb non-climate burdens and supply risk. For industry and policymakers, this translates to practical actions: preferentially adopt powder metallurgy/quick sintering routes, require low-carbon electricity in supplier contracts, implement smelter sourcing standards that control air and water emissions, fund co-product optimization at Cu/Pb refineries to stabilize Te supply, and develop extended producer responsibility (EPR)-style take-back, design-for-recycling, and quality standards for recovered Bi/Te/Sb. Finally, reporting device-level key performance indicators (KPIs) (MJ/kg and kg $CO_2$ per TEG) alongside $\Delta T$, duty cycle, and degradation enables buyers and regulators to benchmark factories and deployments with consistent and actionable metrics. Future research should integrate recycling pathways for critical elements such as Te, consider emerging TE nanocomposite materials with higher efficiency, and assess real-world deployment scenarios to refine energy payback and impact profiles.

### Economic and ethical concerns

While this study establishes a transparent cradle-to-gate baseline for $Bi_2Te_3$-based TEGs, uncertainties remain in scaling laboratory manufacturing energy use to industrial levels and in the exclusion of EoL scenarios. A natural next step is a cradle-to-cradle extension that quantifies the value of closed-loop recovery, particularly for critical elements such as Te and Bi, whose primary extraction dominates several impact categories. Extending to cradle to cradle will require parameterization of collection rates, dismantling and sorting energy and yields (e.g., removal of $Al_2O_3$ plates, Cu leads, and Ni contacts and isolation of TE cores), metallurgical recovery routes and yields for Te/Bi/Sb/Se (e.g., hydrometallurgy vs. pyrometallurgy) together with electricity/fuel and reagent inputs, refining to alloy-grade and quality losses (e.g., closed loop back to TE alloys vs. down-cycling), and the allocation method used to assign recycling credits (e.g., cutoff, 50/50 EoL, or substitution/avoided burden).

Attention should be paid to the environmental and health risks associated with mining legacy and waste. For instance, the Xikuangshan mine (China) is a major Sb producer and exhibits water Sb levels up to two to three orders of magnitude above natural background levels (0.33–11.4 ppm vs. <1 ppb), along with signs of worker intoxication and ecosystem degradation.[56] These contamination pathways merit inclusion in future LCAs through modeling of emissions such as acid mine drainage, arsenic mobilization, and soil pollution, especially in local communities. Mineral extraction and refinement play a central role in regional economies, generating employment, infrastructure, and fiscal revenue. For instance, the Sb sector is a primary local economic driver in Xikuangshan.[57] Future research should also dive into evaluating regional economic growth, benefit sharing, and corporate accountability in relation to TE material acquisition and TEG manufacturing. The risks of informal labor, gender inequality, and unsafe working conditions remain pertinent in the mining sector. It is estimated that less than 10% of the large-scale mining workforce is female globally, with women facing significant pay gaps and discrimination.[58] Embedding fair labor practices, diversity targets, worker safety protocols, and health protections into supply chain standards is essential. Incorporating these metrics into future LCAs or broader sustainability frameworks will help signal social responsibility beyond environmental indicators.

## METHODS

### Environmental LCA

The ISO 14000 environmental management standards (i.e., ISO 14040 and ISO 14044) provide the recognized framework for LCA, described in four phases: goal and scope definition, LCI, life-cycle impact assessment (LCIA), and the interpretation of results.[59,60] Applying this structure to TEG production enables the quantification of energy inputs and emissions, forming the basis for a baseline sustainability profile and for identifying leverage points for improvement.

### Product description

Commercial room temperature TEGs are available in three size ranges: small (100–200 legs), medium (200–500 legs), and large (500–1,000 legs) modules. Typical legs measure 1.5–2 mm in height and 1.5–2.5 $mm^2$ in cross-section.[61] For this study, a representative small-scale module with 150 legs was selected. The legs (1.8 mm length and 2 $mm^2$ cross-section) were sandwiched between alumina wafers ($40 \times 40 \times 1$ $mm^3$).[62] A 0.1-mm-thick Ni contact layer coated the top and bottom of each TE leg to minimize contact resistance with the connectors. The Cu connectors had an area of 6 $mm^2$ and a thickness of 0.3 mm.[63] These components were bonded to the alumina casings with an adhesive, and two external wires were connected to the module for electrical integration. All component masses were calculated using standard bulk densities, as presented in Table 4, with full details provided in Notes S1 and S2.

Please cite this article in press as: Pakdel and Reilly, Life-cycle assessment of carbon footprint and energy intensity of thermoelectric generator production for near-room-temperature applications, Device (2026), https://doi.org/10.1016/j.device.2026.101085





**Table 4. The mass of materials per product unit (i.e., one TEG)**

| | Thermoelectric legs | | | | Metallic connectors | Contact layers | Casings | Adhesive | Wires |
|---|---|---|---|---|---|---|---|---|---|
| | Bi (g) | Te (g) | Sb (g) | Se (g) | Cu (g) | Ni (g) | $Al_2O_3$ (g) | Epoxy (g) | Cu + PVC (g) |
| Type-A TEG | 2.149 | 1.967 | 0.021 | 0.021 | 2.419 | 0.534 | 12.8 | 0.045 | 1.78 + 0.449 |
| Type-B TEG | 1.377 | 1.949 | 0.500 | 0.062 | 2.419 | 0.534 | 12.8 | 0.045 | 1.78 + 0.449 |

## The functional unit

A central aim of this study is to determine the time required for a TEG to generate an amount of energy equivalent to that consumed in its production (EPBT). Accordingly, the functional unit was defined as "1 MJ of electricity generated over the TEG's lifetime." Note S3 summarizes the maximum output power of several commercial $Bi_2Te_3$-based TEGs, deduced from technical datasheets of manufacturers. While a variety of sizes and power ratings are available, the selected values correspond to modules with dimensions and leg counts comparable to those assumed in this study. At small temperature gradients (e.g., $\Delta T$ = 30°C), differences between higher- and lower-powered modules were found to be minimal, but the differences become significant at larger $\Delta T$ values (e.g., $\Delta T$ = 150°C).

For near-room-temperature applications, a $\Delta T$ = 30°C is a reasonable primary assumption. To estimate the power output of type-A TEGs, datasheets from Table S1 (Note S3) were consulted. The power output at $\Delta T$ = 30°C ranges from 0.05 to 0.15 W, leading to an average power of approximately 0.1 W for type-A TEGs in this study. Under continuous operation (24 h/day), this corresponds to approximately 3.153 MJ/year of electricity output, which serves as the reference basis for EPBT calculations.

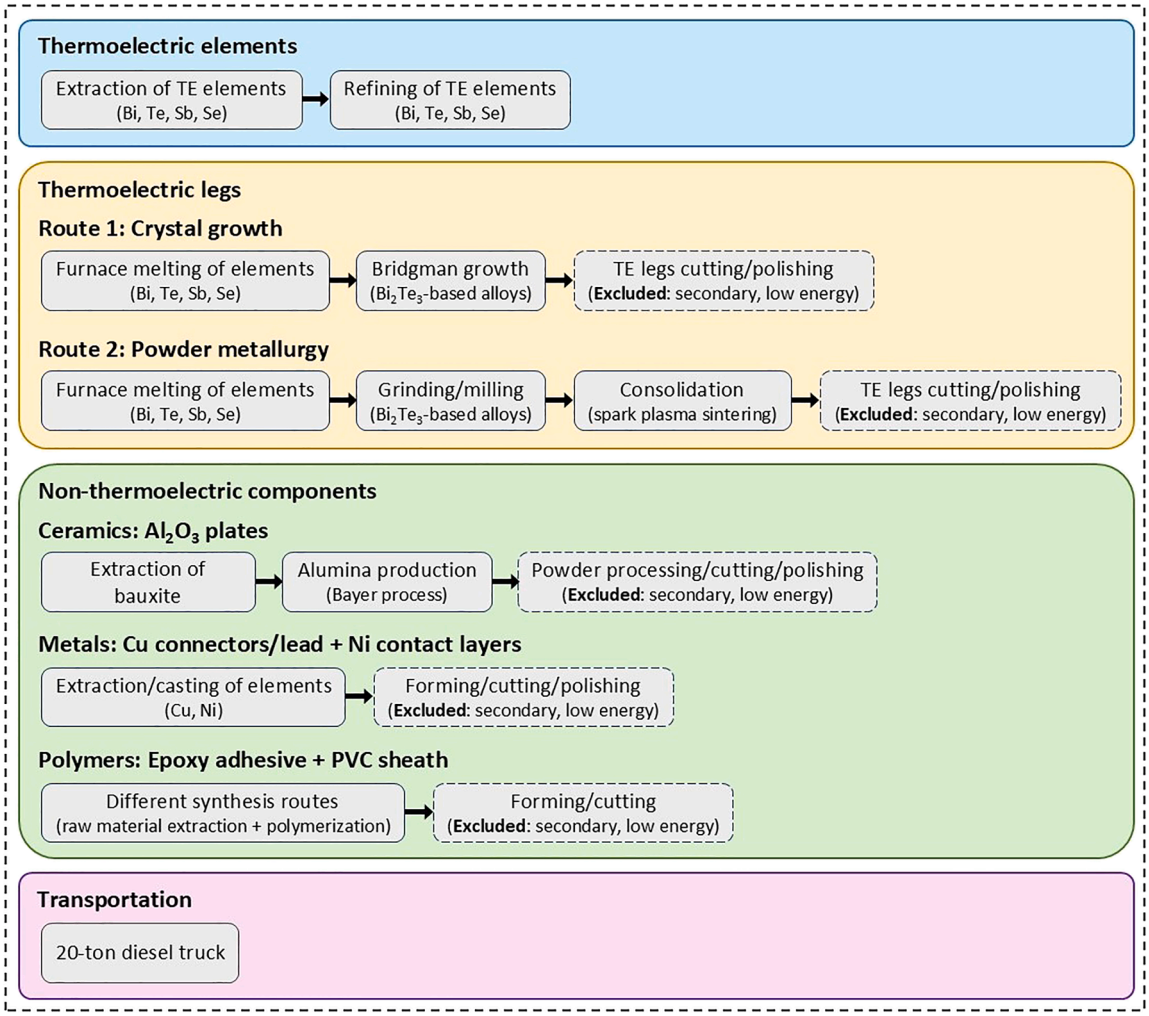


**Figure 5. System boundary and process map for $Bi_2Te_3$-based TEGs studied in the present cradle-to-gate LCA**

Please cite this article in press as: Pakdel and Reilly, Life-cycle assessment of carbon footprint and energy intensity of thermoelectric generator production for near-room-temperature applications, Device (2026), https://doi.org/10.1016/j.device.2026.101085



Type-B TEGs are not yet commercially available and lack datasheet specifications. Their power output was therefore estimated relative to type-A devices: assuming a $ZT_{avg}$ of 1.5 (vs. 1.0 for type A) at $\Delta T = 30^{\circ}C$, resulting in an efficiency increase from ~1.6% to ~2.1%. On this basis, a type-B TEG was estimated to generate ~0.131 W, corresponding to approximately 4.130 MJ/year.

## The system boundaries

Clearly defined system boundaries are essential in LCA to prevent excessive detail and maintain focus. The boundaries applied in this study are as follows.

(1) A cradle-to-gate approach was adopted, covering raw material extraction and refining, TE material synthesis (crystal growth and powder metallurgy), production of non-TE components, and outbound transport to the assembly gate (see LCI). Use-phase and EoL were excluded. EPBT and CPBT were reported as scenario-based indicators, comparing production inventory with assumed operating conditions ($\Delta T$ and duty cycle)—they did not expand the system boundary.
(2) The p- and n-type TE materials used in type-A and type-B TEGs consisted of four elements: Bi, Te, Se, and Sb. Among them, Bi, Se, and Te are by-products of Cu or Pb refining. Therefore, the life cycle of these materials began with Cu or Pb production. By contrast, Sb is directly extracted from stibnite ore; thus, its life cycle started with stibnite mining.
(3) In addition to the TE elements, the analysis included non-TE components such as Ni contact layers, Cu interconnects and wires, $Al_2O_3$ ceramic casings, epoxy adhesives, and polymer sheathing, with masses taken from the product description.
(4) EoL processes (collection, dismantling, recovery, and disposal) were not modeled due to the absence of standardized industrial routes and consistent datasets for $Bi_2Te_3$-based modules. A brief description of the data needs for a future cradle-to-cradle extension is provided in the conclusion and outlook section.
(5) Secondary fabrication steps such as wire drawing, ceramic cutting, adhesive curing, and final module assembly are low-temperature/low-energy processes as compared to extraction, refining, and high-temperature synthesis routes. On a per-unit basis, they are expected to be well below the uncertainty of the dominant processes; therefore, they were excluded from the quantitative boundary.

The system boundaries and process map for the cradle-to-gate LCA of $Bi_2Te_3$-based TEGs are summarized in Figure 5.

## LCI for materials extraction, synthesis, and processing

The LCI was constructed by dividing TEG production into TE materials, non-TE components, and device-level processing steps. For TE materials, the inventory accounts for the extraction and refining of key constituent elements (Bi, Te, Sb, and Se), followed by TE material compound synthesis and processing via two representative and widely adopted routes: conventional crystal growth and powder-metallurgy-based consolidation. Non-TE components, including metallic interconnects, ceramic substrates, polymeric materials, and resins, were modeled using established industrial production pathways. Energy and material flows were compiled from a combination of peer-reviewed literature, industrial reports, and standard LCA databases and normalized to functional units consistent with device-level analysis.

To maintain conciseness, detailed descriptions of individual extraction routes, furnace operating conditions, batch sizes, and energy calculations are provided in Notes S4–S6, together with the full set of LCI parameters and data sources used in this study. A summary of the corresponding data is presented in Table 5.

**Table 5. Inventory data on thermoelectric element extraction, thermoelectric material processing, and non-thermoelectric component extraction and processing**

| | Process description | CED (MJ/kg) |
|---|---|---|
| TE element | | |
| Antimony (Sb) | stibnite ore mining, smelting, reduction | 141 |
| Bismuth (Bi) | by-product of Pb refining (Kroll-Betterton process) | 697 |
| Tellurium (Te) | by-product of Cu refining (soda roasting and acid leaching) | 435 |
| Selenium (Se) | by-product of Cu refining (soda roasting and water leaching) | 66 |
| TE material synthesis process | | |
| Crystal growth | Bridgman method | 1730 |
| Powder metallurgy | furnace melting and solidification (using a vacuumed quartz tube) | 150 |
| | ball milling | 360 |
| | spark plasma sintering | 280 |
| Non-TE component | | |
| Copper (Cu) | extraction from sulfide ores, refining (leaching and smelting) | 54 |
| Nickel (Ni) | extraction from laterite/sulfide ores, refining (leaching and smelting) | 111 |
| Alumina ($Al_2O_3$) | extraction from bauxite (Bayer process) | 7 |
| Epoxy resin | polymerization of BPA and ECH (derived from petrochemical feedstocks) | 107 |
| Polyvinyl chloride | chlorination of ethylene, thermal cracking | 53 |

## LCI for transportation

The transportation phase was modeled using a 20-ton diesel-fueled truck, consistent with options available in the GaBi database. A transport distance of 1,800 km was assumed, corresponding to the overland route between the Caijiaying mine in Hebei Province (a major Bi source) and the Thermonamic TEG facility in Jiangxi Province (a leading $Bi_2Te_3$ TEG producer). For simplicity, transport was treated as a single step from extraction to manufacturing.

Energy use was allocated proportionally to the mass of TE material per TEG relative to the truck's full load capacity, as summarized in Note S7. The calculated CED for transportation of type-A and type-B TEGs was ≈0.0075 (MJ) and ≈0.0070 (MJ), respectively.

## ACKNOWLEDGMENTS

The authors are grateful to Dr. Karina Vink (University of Twente) for fruitful discussions.

## DECLARATION OF INTERESTS

The authors declare no competing interests.

## SUPPLEMENTAL INFORMATION

Supplemental information can be found online at https://doi.org/10.1016/j.device.2026.101085.

## REFERENCES

1. Gayner, C., and Kar, K.K. (2016). Recent advances in thermoelectric materials. Prog. Mater. Sci. *83*, 330–382. https://doi.org/10.1016/j.pmatsci.2016.07.002.
2. DiSalvo, F.J. (1999). Thermoelectric Cooling and Power Generation. Science *285*, 703–706. https://doi.org/10.1126/science.285.5428.703.
3. Tritt, T.M. (2011). Thermoelectric Phenomena, Materials, and Applications. Annu. Rev. Mater. Res. *41*, 433–448. https://doi.org/10.1146/annurev-matsci-062910-100453.
4. Poudel, B., Hao, Q., Ma, Y., Lan, Y., Minnich, A., Yu, B., Yan, X., Wang, D., Muto, A., Vashaee, D., et al. (2008). High-Thermoelectric Performance of Nanostructured Bismuth Antimony Telluride Bulk Alloys. Science *320*, 634–638. https://doi.org/10.1126/science.1156446.
5. Zhang, C., de la Mata, M., Li, Z., Belarre, F.J., Arbiol, J., Khor, K.A., Poletti, D., Zhu, B., Yan, Q., and Xiong, Q. (2016). Enhanced thermoelectric performance of solution-derived bismuth telluride based nanocomposites via liquid-phase Sintering. Nano Energy *30*, 630–638. https://doi.org/10.1016/j.nanoen.2016.10.056.
6. Liu, C.-J., Lai, H.C., Liu, Y.-L., and Chen, L.-R. (2012). High thermoelectric figure-of-merit in p-type nanostructured (Bi,Sb)2Te3 fabricated viahydrothermal synthesis and evacuated-and-encapsulated sintering. J. Mater. Chem. *22*, 4825–4831. https://doi.org/10.1039/C2JM15185E.
7. Kato, K., Hatasako, Y., Uchino, M., Nakata, Y., Suzuki, Y., Hayakawa, T., Adachi, C., and Miyazaki, K. (2014). Flexible Porous Bismuth Telluride Thin Films with Enhanced Figure of Merit using Micro-Phase Separation of Block Copolymer. Adv. Mater. Interfaces *1*, 1300015. https://doi.org/10.1002/admi.201300015.
8. Li, Y.Y., Qin, X.Y., Li, D., Zhang, J., Li, C., Liu, Y.F., Song, C.J., Xin, H.X., and Guo, H.F. (2016). Enhanced thermoelectric performance of Cu2Se/Bi0.4Sb1.6Te3 nanocomposites at elevated temperatures. Appl. Phys. Lett. *108*, 062104. https://doi.org/10.1063/1.4941757.
9. Chen, S., Logothetis, N., Ye, L., and Liu, J. (2015). A High Performance Ag Alloyed Nano-scale n-type Bi2Te3 Based Thermoelectric Material. Mater. Today Proc. *2*, 610–619. https://doi.org/10.1016/j.matpr.2015.05.083.
10. Kim, J., Duy, L.T., Ahn, B., and Seo, H. (2020). Pre-oxidation effects on properties of bismuth telluride thermoelectric composites compacted by spark plasma sintering. Journal of Asian Ceramic Societies *8*, 211–221. https://doi.org/10.1080/21870764.2020.1723197.
11. Shin, W.H., Roh, J.W., Ryu, B., Chang, H.J., Kim, H.S., Lee, S., Seo, W.S., and Ahn, K. (2018). Enhancing Thermoelectric Performances of Bismuth Antimony Telluride via Synergistic Combination of Multiscale Structuring and Band Alignment by FeTe2 Incorporation. ACS Appl. Mater. Interfaces *10*, 3689–3698. https://doi.org/10.1021/acsami.7b18451.
12. Zheng, X.F., Liu, C.X., Yan, Y.Y., and Wang, Q. (2014). A review of thermoelectrics research – Recent developments and potentials for sustainable and renewable energy applications. Renew. Sustain. Energy Rev. *32*, 486–503. https://doi.org/10.1016/j.rser.2013.12.053.
13. Zhang, X., and Zhao, L.-D. (2015). Thermoelectric materials: Energy conversion between heat and electricity. J. Materiomics *1*, 92–105. https://doi.org/10.1016/j.jmat.2015.01.001.
14. Lv, H.Y., Liu, H.J., Shi, J., Tang, X.F., and Uher, C. (2013). Optimized thermoelectric performance of Bi2Te3 nanowires. J. Mater. Chem. A Mater. *1*, 6831–6838. https://doi.org/10.1039/C3TA10804J.
15. Hicks, L.D., and Dresselhaus, M.S. (1993). Effect of quantum-well structures on the thermoelectric figure of merit. Phys. Rev. B *47*, 12727–12731. https://doi.org/10.1103/PhysRevB.47.12727.
16. Venkatasubramanian, R., Siivola, E., Colpitts, T., and O'Quinn, B. (2001). Thin-film thermoelectric devices with high room-temperature figures of merit. Nature *413*, 597–602. https://doi.org/10.1038/35098012.
17. Kawajiri, K., Kishita, Y., and Shinohara, Y. (2021). Life Cycle Assessment of Thermoelectric Generators (TEGs) in an Automobile Application. Sustainability *13*, 13630. https://doi.org/10.3390/su132413630.
18. Kishita, Y., Ohishi, Y., Uwasu, M., Kuroda, M., Takeda, H., and Hara, K. (2016). Evaluating the life cycle CO2 emissions and costs of thermoelectric generators for passenger automobiles: a scenario analysis. J. Clean. Prod. *126*, 607–619. https://doi.org/10.1016/j.jclepro.2016.02.121.
19. Lupu, A.G., Homutescu, V.M., Bălănescu, D.T., and Popescu, A. (2020). Hybrid PV-TE-T modules: life cycle analysis and end of life assessment. IOP Conf. Ser. Mater. Sci. Eng. *997*, 012149. https://doi.org/10.1088/1757-899X/997/1/012149.
20. Lekbir, A., Hassani, S., and Mekhilef, S. (2024). Techno-economic and life cycle assessment of a nanofluid-based concentrated Photovoltaic/Thermal-Thermoelectric hybrid system. J. Power Sources *595*, 234066. https://doi.org/10.1016/j.jpowsour.2024.234066.
21. Li, W., Kan, J., Zhao, W., Wang, J., Zhang, X., and Zhao, J. (2024). Economic and life cycle analysis of a photovoltaic thermal application system based on phase change thermal storage. Appl. Therm. Eng. *257*, 124261. https://doi.org/10.1016/j.applthermaleng.2024.124261.
22. Rahman, S.M.A., Hachicha, A.A., Ghenai, C., Saidur, R., and Said, Z. (2020). Performance and life cycle analysis of a novel portable solar thermoelectric refrigerator. Case Stud. Therm. Eng. *19*, 100599. https://doi.org/10.1016/j.csite.2020.100599.
23. Bozorgi, M., Roy, P., Siddique, A.R.M., Venkateshwar, K., Tasnim, S., and Mahmud, S. (2023). Experimental investigation and life cycle assessment of a phase change material (PCM) based thermoelectric (TE) refrigerator. Int. J. Thermofluids *19*, 100394. https://doi.org/10.1016/j.ijft.2023.100394.
24. Zhu, H., Deng, Z., Qu, Y., He, P., and Geng, H. (2025). Strong texture in nanostructured bulk Bi0.5Sb1.5Te3 leads to superior thermoelectric and mechanical performance. J. Mater. Sci. Technol. *232*, 267–275. https://doi.org/10.1016/j.jmst.2024.12.086.
25. Pang, K., Miao, L., Zhang, Q., Pan, Q., Liu, Y., Shi, H., Li, J., Zhou, W., Zhang, Z., Zhang, Y., et al. (2024). Gradient Nanotwins and Enhanced Weighted Mobility Synergistically Upgrade Bi0.5Sb1.5Te3 Thermoelectric and Mechanical Performance. Adv. Funct. Mater. *34*, 2315591. https://doi.org/10.1002/adfm.202315591.
26. Boz, R.B., Sevik, C., and Turan, S. (2025). Improving the power factor of spark plasma sintered Bi0,5Sb1,5Te3 via TiC dispersion. J. Alloys Compd. *1010*, 177917. https://doi.org/10.1016/j.jallcom.2024.177917.
27. Shen, J.-J., Zhu, T.-J., Zhao, X.-B., Zhang, S.-N., Yang, S.-H., and Yin, Z.-Z. (2010). Recrystallization induced in situ nanostructures in bulk bismuth antimony tellurides: a simple top down route and improved thermoelectric properties. Energy Environ. Sci. *3*, 1519–1523. https://doi.org/10.1039/C0EE00012D.

28. Zhu, T., Xu, Z., He, J., Shen, J., Zhu, S., Hu, L., Tritt, T.M., and Zhao, X. (2013). Hot deformation induced bulk nanostructuring of unidirectionally grown p-type (Bi,Sb)2Te3 thermoelectric materials. J. Mater. Chem. A Mater. *1*, 11589–11594. https://doi.org/10.1039/C3TA12764H.

29. Cook, B.A., Chan, T.E., Dezsi, G., Thomas, P., Koch, C.C., Poon, J., Tritt, T., and Venkatasubramanian, R. (2015). High-Performance Three-Stage Cascade Thermoelectric Devices with 20% Efficiency. J. Electron. Mater. *44*, 1936–1942. https://doi.org/10.1007/s11664-014-3600-9.

30. Chen, C.-L., Wang, T.-H., Yu, Z.-G., Hutabalian, Y., Vankayala, R.K., Chen, C.-C., Hsieh, W.-P., Jeng, H.-T., Wei, D.-H., and Chen, Y.-Y. (2022). Modulation Doping Enables Ultrahigh Power Factor and Thermoelectric ZT in n-Type Bi2Te2.7Se0.3. Adv. Sci. *9*, 2201353. https://doi.org/10.1002/advs.202201353.

31. Zhang, W., Liu, X., Tian, Z., Zhang, Y., Li, X.-J., and Song, H. (2023). High Thermoelectric Performance of Large Size Bi2Te2.7Se0.3 Alloy Ingots. J. Electron. Mater. *52*, 6682–6689. https://doi.org/10.1007/s11664-023-10590-9.

32. Diao, J., Yuan, J., Cai, Z., Xia, L., Cheng, Z., Liu, X., Ma, W., Wang, S., and Huang, Y. (2022). High-performance electromagnetic interference shielding and thermoelectric conversion derived from multifunctional Bi2Te2.7Se0.3/MXene composites. Carbon *196*, 243–252. https://doi.org/10.1016/j.carbon.2022.04.078.

33. Wu, G., Tan, X., Yuan, M., Zhang, Q., Noudem, J.G., Liu, Z., Cui, C., Wu, J., Hu, H., Sun, P., et al. (2023). High thermoelectric and mechanical performance in strong-textured n-type Bi2Te2.7Se0.3 by temperature gradient method. Chem. Eng. J. *470*, 144085. https://doi.org/10.1016/j.cej.2023.144085.

34. Hu, Q., Guo, J., Zhao, X., Guan, C., Wang, S., and Zhao, Z. (2024). Enhanced thermoelectric properties of 3D printed Bi2Te2.7Se0.3 by atomic interface engineering. J. Alloys Compd. *1004*, 175770. https://doi.org/10.1016/j.jallcom.2024.175770.

35. Kim, S.I., Lee, K.H., Mun, H.A., Kim, H.S., Hwang, S.W., Roh, J.W., Yang, D.J., Shin, W.H., Li, X.S., Lee, Y.H., et al. (2015). Dense dislocation arrays embedded in grain boundaries for high-performance bulk thermoelectrics. Science *348*, 109–114. https://doi.org/10.1126/science.aaa4166.

36. Başar Boz, R., Sevik, C., and Turan, S. (2025). Enhanced thermoelectric performance of Bi0.5Sb1.5Te3 alloys via amorphous glass particle integration. Mater. Sci. Eng., B *321*, 118544. https://doi.org/10.1016/j.mseb.2025.118544.

37. Chen, H., Luo, K., Qian, P., Deng, Y., Li, A., Sun, Q., Yang, L., Liu, Y., Wang, Z., Ren, G.-K., et al. (2025). Promoting Room-Temperature n-type Bismuth Telluride Thermoelectrics via High-Potential Barrier Heterointerfaces. ACS Appl. Mater. Interfaces *17*, 18800–18812. https://doi.org/10.1021/acsami.5c01400.

38. Yen, W.-T., Huang, H.-C., Wang, K.-K., and Wu, H.-J. (2021). Nano-precipitation and carrier optimization synergistically yielding high-performance n-type Bi2Te3 thermoelectrics. Mater. Today Phys. *19*, 100416. https://doi.org/10.1016/j.mtphys.2021.100416.

39. Masoumi, S., and Pakdel, A. (2022). Nanoengineering Approaches to Tune Thermal and Electrical Conductivity of a BiSbTe Thermoelectric Alloy. Adv. Eng. Mater. *24*, 2100955. https://doi.org/10.1002/adem.202100955.

40. Chen, F., Lei, J., Liu, Z., and Xiong, X. (2025). A Comparative Study on the Average CO2 Emission Factors of Electricity of China. Energies *18*, 654. https://doi.org/10.3390/en18030654.

41. (2019). Guidance on measuring and reporting Greenhouse Gas (GHG) emissions from freight transport operations. https://www.gov.uk/guidance/measuring-and-reporting-environmental-impacts-guidance-for-businesses.

42. (2025). Greenhouse gas reporting: conversion factors 2025. https://www.gov.uk/government/collections/government-conversion-factors-for-company-reporting?utm_source=chatgpt.com.

43. Ou, X., Xiaoyu, Y., and Zhang, X. (2011). Life-cycle energy consumption and greenhouse gas emissions for electricity generation and supply in China. Appl. Energy *88*, 289–297. https://doi.org/10.1016/j.apenergy.2010.05.010.

44. (2025). IEA World Energy Statistics and Balances. https://www.iea.org/data-and-statistics/data-product/world-energy-statistics-and-balances.

45. (2025). Installed electricity generation capacity in China from 2011 to 2024, by source. https://www.statista.com/statistics/302191/china-power-generation-installed-capacity-by-source/.

46. Tukker, A., and Jansen, B. (2006). Environmental Impacts of Products: A Detailed Review of Studies. J. Ind. Ecol. *10*, 159–182. https://doi.org/10.1162/jiec.2006.10.3.159.

47. Nuss, P., and Eckelman, M.J. (2014). Life Cycle Assessment of Metals: A Scientific Synthesis. PLoS One *9*, e101298. https://doi.org/10.1371/journal.pone.0101298.

48. Graedel, T.E., Harper, E.M., Nassar, N.T., Nuss, P., and Reck, B.K. (2015). Criticality of metals and metalloids. Proc. Natl. Acad. Sci. USA *112*, 4257–4262. https://doi.org/10.1073/pnas.1500415112.

49. (2025). Mineral commodity summaries 2025. Report 2025. https://pubs.usgs.gov/publication/mcs2025.

50. Goedkoop, M., Heijungs, R., Huijbregts, M., Schryver, A., Struijs, J., and Zelm, R. (2008). ReCiPE 2008: A life cycle impact assessment method which comprises harmonised category indicators at the midpoint and the endpoint level (The Ministry of Housing and Spatial Planning (VROM)). https://www.rivm.nl/en/life-cycle-assessment-lca/recipe.

51. Steinboeck, A., Wild, D., and Kugi, A. (2013). Energy-Efficient Control of Continuous Reheating Furnaces. IFAC Proc. Vol. *46*, 359–364. https://doi.org/10.3182/20130825-4-US-2038.00007.

52. (2016). Improving Process Heating System Performance V3 (EERE Publication and Product Library). https://www.osti.gov/biblio/1247916.

53. Hamawandi, B., Batili, H., Paul, M., Ballikaya, S., Kilic, N.I., Szukiewicz, R., Kuchowicz, M., Johnsson, M., and Toprak, M.S. (2021). Minute-Made, High-Efficiency Nanostructured Bi(2)Te(3) via High-Throughput Green Solution Chemical Synthesis. Nanomaterials *11*, 2053. https://doi.org/10.3390/nano11082053.

54. Zhang, Z., Sun, M., Liu, J., Cao, L., Su, M., Liao, Q., Deng, Y., and Qin, L. (2022). Ultra-fast fabrication of Bi2Te3 based thermoelectric materials by flash-sintering at room temperature combining with spark plasma sintering. Sci. Rep. *12*, 10045. https://doi.org/10.1038/s41598-022-14405-5.

55. Zhao, J., Ma, L., Zayed, M.E., Elsheikh, A.H., Li, W., Yan, Q., and Wang, J. (2021). Industrial reheating furnaces: A review of energy efficiency assessments, waste heat recovery potentials, heating process characteristics and perspectives for steel industry. Process Saf. Environ. Prot. *147*, 1209–1228. https://doi.org/10.1016/j.psep.2021.01.045.

56. Liu, F., Le, X.C., McKnight-Whitford, A., Xia, Y., Wu, F., Elswick, E., Johnson, C.C., and Zhu, C. (2010). Antimony speciation and contamination of waters in the Xikuangshan antimony mining and smelting area, China. Environ. Geochem. Health *32*, 401–413. https://doi.org/10.1007/s10653-010-9284-z.

57. Hao, W., Liu, H., Hao, S., and Mao, K. (2024). Characterization of heavy metal contamination in groundwater of typical mining area in Hunan Province. Sci. Rep. *14*, 13054. https://doi.org/10.1038/s41598-024-63460-7.

58. Rahimpour, S., El-Wali, M., Makarava, I., Tuomisto, H.L., Lundström, M., and Kraslawski, A. (2024). Selected social impact indicators influenced by materials for green energy technologies. Nat. Commun. *15*, 9336. https://doi.org/10.1038/s41467-024-53652-0.

59. International Organization for Standardization (2006). Environmental Management — Life Cycle Assessment — Principles and Framework (ISO 14040:2006).

60. International Organization for Standardization (2006). Environmental Management — Life Cycle Assessment — Requirements and Guidelines (ISO 14044:2006).

61. Lee, K.-T., Lee, D.-S., Chen, W.-H., Lin, Y.-L., Luo, D., Park, Y.-K., and Bandala, A. (2023). An overview of commercialization and marketization of thermoelectric generators for low-temperature waste heat recovery. iScience *26*, 107874. https://doi.org/10.1016/j.isci.2023.107874.

62. Van Toan, N., Tuoi, T.T.K., and Ono, T. (2020). Thermoelectric generators for heat harvesting: From material synthesis to device fabrication. Energy Convers. Manag. *225*, 113442. https://doi.org/10.1016/j.enconman.2020.113442.

63. Sun, W., Sui, R., Yuan, G., Zheng, H., Zeng, Z., Xie, P., Yuan, L., Ren, Z., Cai, F., and Zhang, Q. (2021). Thermoelectric module design to improve lifetime and output power density. Mater. Today Phys. *18*, 100391. https://doi.org/10.1016/j.mtphys.2021.100391.